A blind test on wind turbine wake modelling: Benchmark results and Phase II announcement

I Chondromatidis[1], V Pappa[1], B S Dsouza[2], A Sciacchitano[2], S Tamaro[3], F V Mühle[3], F Campagnolo[3] and M Manolesos[1]

[1] School of Mechanical Engineering, National Technical University of Athens, Athens, Greece
[2] Aerospace Engineering, Delft University of Technology, Delft, the Netherlands
[3] Wind Energy Institute, Technical University of Munich, Munich, Germany

*E-mail: marinos@fluid.mech.ntua.gr

Abstract. Accurate modelling of wind turbine wakes is critical for optimizing wind farm performance, but the complexity of wake interactions poses significant challenges. This study presents a two-phase blind test campaign, part of the Horizon Europe TWEET-IE project, designed to benchmark numerical models and investigate wake control strategies using wind tunnel experiments. Conducted with tandem wind turbine models at the Technical University of Munich and the National Technical University of Athens, the tests include inflow, load, power, and wake velocity measurements under controlled conditions. Phase I serves as an open-data benchmarking exercise for a baseline scenario without wake control, while Phase II introduces active individual blade pitch control to the upstream turbine, challenging participants to simulate advanced wake dynamics. This paper reviews Phase I results and details the experimental framework for Phase II, providing a foundation for advancing wake modelling and control in wind energy research.

1. Introduction

As the wind energy industry continues to grow, optimizing wind farm design and operation becomes increasingly important. Accurate modelling of wind turbine wakes is a key aspect, as these wakes and their interactions significantly influence energy production, turbine placement, and operational strategies. However, capturing the complexity of turbine wakes remains a challenging task due to the intricate interplay between wake dynamics, atmospheric boundary layer behaviour, and wind farm configurations [1]. Additionally, implementing effective wake control strategies can dramatically enhance a wind farm's energy output while reducing the levelized cost of energy, thereby improving the financial viability of wind energy projects. Achieving these outcomes relies on precise wake modelling to identify optimal control methods and operational practices [2].

Several studies have been conducted to improve the understanding of wind turbine wake dynamics through a series of "Blind Test" workshops. The first Blind Test (BT1) by Krogstad and Eriksen [3] investigated wake development up to 5 rotor diameters downstream of a single wind turbine, revealing modeling challenges in predicting wake behavior. BT2 introduced a downstream turbine in the wake of an upstream turbine, demonstrating increased complexity in

wake interactions. Subsequently, BT3 examined the effects of a lateral offset between two turbines, highlighting the asymmetric wake impact on the downstream turbine. BT4 analyzed wake behavior under different turbulence conditions, providing insights into atmospheric inflow effects on wake recovery. Finally, BT5 explored the wake flow and performance of yawed wind turbines, showing that power predictions for a single yawed turbine varied by ±19%, while downstream turbine predictions in partial wake conditions exhibited a much larger scatter of ±49%, emphasizing the challenges in modeling dynamic wake effects [4].

Building on these challenges, the present paper expands upon previous work [5], presenting a new blind test on wind turbine wake modelling and control, introducing individual pitch control for wake manipulation for the first time. A two-phase blind test study was designed to advance the field of wake modelling. The blind test initiative aims at enhancing wake modelling accuracy by benchmarking numerical models against open experimental data, improving confidence in wake modelling methodologies. Initially introduced at the TORQUE 2024 conference, the blind test seeks to evaluate numerical approaches, quantify uncertainties, and foster transparency and collaboration within the wind energy community.

To support this initiative, two experimental campaigns were performed at Technische Universität München (TUM) and at the National Technical University of Athens (NTUA) to investigate wake flow control techniques. This document will briefly discuss the experimental set up and results and will present the relevant comparisons with the numerical predictions provided by the participants of Phase I. While both experimental set ups are detailed, only data from the TUM campaign are available at the time of writing, as the NTUA campaign results will form Phase II of an ongoing blind test campaign[1] and cannot currently be published. The details of the two distinct phases are below.

- ✓ **Phase I: Benchmark Case**
  This phase invites participants to simulate a baseline case involving two aligned turbines without active wake control. The objective is to establish a reference dataset for numerical model validation, ensuring participants can benchmark their approaches against experimental results. Open data for this phase are accessible at https://doi.org/10.5281/zenodo.10566400.
- ✓ **Phase II: Blind Test**
  This phase presents a more complex scenario, where the upstream turbine's wake is controlled using active individual blade pitch. While the case specifications (e.g., inflow conditions, turbine geometry, wake control strategy) are provided, the experimental results are withheld.

2. Phase I – Experiment Description

Phase I experiments were conducted in the closed-loop, low-speed boundary layer wind tunnel at TUM. The set up consists of two identically scaled wind turbine models, placed in line with a longitudinal distance of 5D, where D denotes the rotor's diameter. Figure 1 represents the experimental setup at TUM, showing the static pressure taps located at the centre (y=0) of the

[1] http://www.tweet-ie.eu/Blind_Test

wind tunnel ceiling, the location of the pitot tube as well as the wind turbine models. The inflow conditions of the experiment, measured at both positions, are shown in Figure 2.

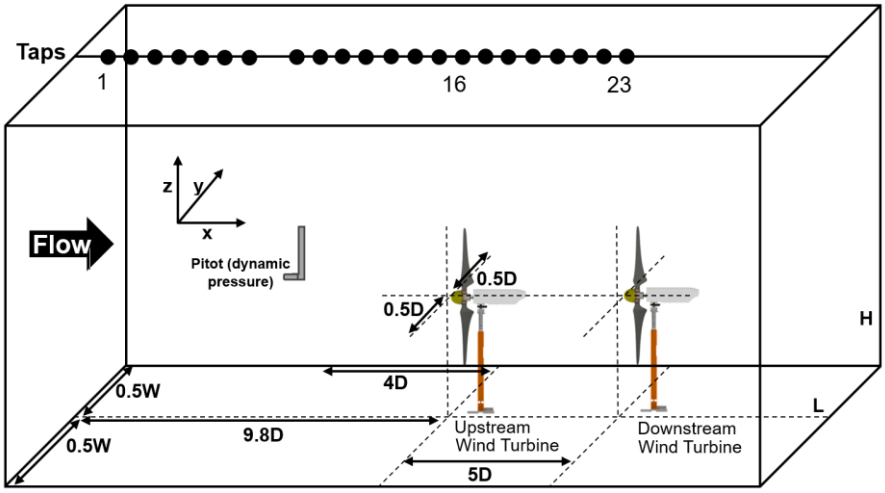

Figure 1. Sketch of the wind tunnel test section at TUM with the positioning of the pressure taps in the centre of the wind tunnel ceiling, the location of the pitot tube and the locations of the upstream and downstream wind turbine models.

The turbine models used were the G1 turbines [6], developed by TUM, designed for precise performance characterization and equipped with advanced sensors for measuring torque, thrust, and other performance metrics. A detailed picture of the G1 turbine can be seen in Figure 3, while the chord and twist distributions are given in Figure 4. G1 features a rotor diameter of $D = 1.1$ m, a hub height of $z_{hub} = 0.82$ m, a rated rotor speed, $\omega = 850$ rpm (CW rotation) and a blade pitch $\beta \approx 0.4°$. The airfoil polars of the turbine were also provided by the manufacturer, taking the Reynolds number into consideration. Presented experimental data have not been corrected for blockage and CFD simulations are expected to model the Wind Tunnel wall effects.

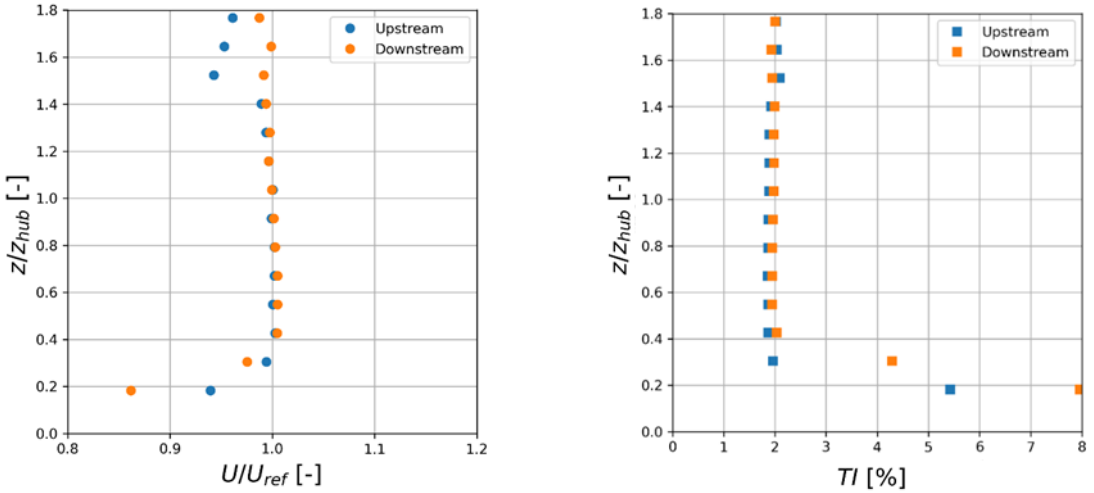

Figure 2. Normalized velocity (left) and turbulence intensity (right) per normalized height for the Phase I experiment conducted at TUM.

For all cases, the turbine power coefficient, $\mathbf{C_P}$, was calculated using equation 2.1

$$C_P = \frac{P}{0.5\rho U_{pitot}^3 \pi (0.5D)^2} = \frac{\omega T}{0.5\rho U_{pitot}^3 \pi (0.5D)^2} \quad (2.1)$$

where P is the power, ω is the rotor speed, T is the torque measured by the shaft strain gauges and U_{pitot} is the uncorrected wind tunnel velocity, measured with the pitot tube located at hub height, 50cm from the tunnel side wall in a distance of 4D upwind of the upstream wind turbine model. The thrust coefficient, C_T, was calculated using equation 2.2 and finally, the Tip Speed Ratio (TSR) was calculated using equation 2.3:

$$C_T = \frac{Thrust}{0.5\rho U_{pitot}^2 \pi (0.5D)^2} \quad (2.2)$$

$$TSR = \frac{\omega D}{2U_{pitot}} \quad (2.3)$$

Figure 3. The G1 wind turbine with highlighted components.

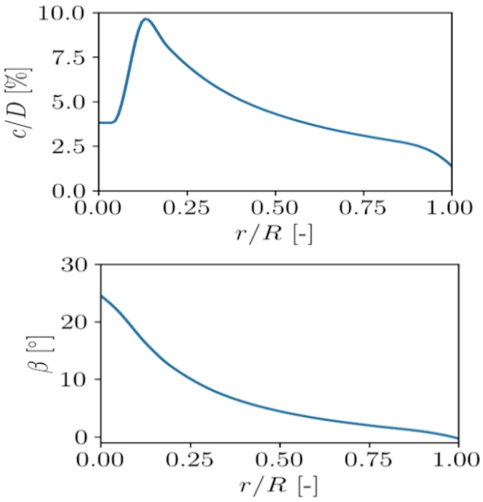

Figure 4. Chord and twist distribution for the G1 wind turbine model.

3. Numerical Approaches

With the Phase I deadline of the blind test campaign still ongoing at the time of writing, five institutions have contributed their numerical simulations for comparison with the experimental measurements. To ensure impartiality in the audience's evaluation, the authors have chosen to anonymize the contributors' identities. Consequently, each institution is referred to as *"Participant #"*, where # denotes the corresponding institution's number.

Participant 1 utilizes a computationally cheap in-house C-code based on the Blade Element Theory (BET), incorporating the free vortex wake model. In the latter, the rotating blades are modelled with **N** number of blade elements along the blade span. $\mathbf{N+1}$ vortex filaments are shed from the blades at each time step of the unsteady rotor simulation, allowing for any prescribed rotor motion. The model implements straight-line vortex discretization, which divides a vortex filament into short straight vortex line segments. The velocity induced by each vortex line segment is computed using the Biot-Savart law [7]. The core radius $\mathbf{r_c}$ of the vortex filaments is determined using the growth model [8], which explains the variation of the vortex core radius as a function of wake age $\boldsymbol{\psi_w}$. Neither the wind tunnel walls, nor the nacelle is modelled in this approach.

Participant 2 employs an in-house compressible cell-centred URANS solver, coupled with the k-ω SST turbulence model. The rotor blades of the wind turbines are modelled with the Actuator Line Method (ALM), whilst the tower and nacelle of the turbines are excluded. The blade loads are computed at specific control points along the blade span through BET in conjunction with tabulated 2D polars. The aerodynamic forces at the control points are then applied to the flow as source terms in the flow equations, distributed across the mesh cells swept by the blades during their rotation [9]. In order to resolve the boundary layer a grid refinement was made close to the walls of the wind tunnel, setting the distance of the 1st node from the wall at 0.001m and using a geometrical progress ratio of 1.2. The computational mesh is unstructured and consists of approximately 8.5×10^6 cells.

Participant 3 solves the unsteady, incompressible Navier-Stokes equations using an open source CFD solver incorporating a LES approach combined with the ALM of 100 points per blade. Second-order centred spatial and second-order backward temporal discretisation schemes were used, along with the PISO algorithm for pressure-velocity coupling. The standard Smagorinsky turbulence model was employed, as subgrid-scale turbulence generally does not significantly impact ALM-LES predictions of wind turbine wakes, provided that the computational mesh is sufficiently well refined [10]. The mesh consists of $\sim$ 20 million cells. All four wind tunnel walls are simulated with a symmetry boundary condition for U and p. The wind tunnel wall boundary layer is therefore neither resolved nor modelled. The nacelle walls are simulated using an analytical wall function. The nacelle mesh is characterised by y^+ values of the order of $y^+ \approx 300$.

Participant 4 employs an in-house LES model using the Finite Volume Method (FVM) with high-order numerical schemes. Their solver is based on the filtered Navier-Stokes equations for incompressible fluid flow and utilizes a prediction-correction technique on an Eulerian grid. Slip wall boundary conditions are imposed on the domain's top, bottom and side walls to consider the confinement effect without solving the boundary layers, while the nacelle is excluded from the geometry. The Smagorinsky model is applied to represent sub-grid scale turbulent fluxes, using a coefficient of $C_S = 0.16$. An unstructured mesh consisting of 120×10^6 tetrahedra is used, achieving a resolution of $\Delta x \approx 12.5$ mm (or $D/\Delta x = 88$) within a refinement region of 1.25D in diameter, encompassing both the turbines and its wake downstream. The rotor is modelled with the ALM using 64 actuator points per blade and the forces were projected onto the Eulerian grid using the isotropic Gaussian function.

Participant 5 uses an in-house version of an open-source software, consisting of a FVM LES solver based on the standard PISO incompressible formulation. They apply a standard Smagorinsky subgrid scales model with a constant of $C_S = 0.16$. The wind turbine model's blades are modelled using the ALM with 108 points per blade, with the velocity sampling approach of [11] and the smearing correction of the tip forces by [12]. The orthogonal mesh consists of approximately 28×10^6 cells and presents the finest cell size of 0.01 m in correspondence with the rotor. The inflow is generated using a synthetic turbulence generation method. The wind tunnel walls are simulated through inviscid fluid flow and the nacelle's geometry is included in the simulation.

The complete list of participant models and their descriptions can be found in Table 1.

Table 1. List of Phase I participants' models.

#	Sim. Type	Solver	Wind Tunnel Walls	Nacelle Modelling	Turb. Modelling	Mesh	WT Modelling	Cost (1:lowest 5:highest)
1	BET	In-house	No	No	-	-	Free vortex	1
2	URANS	In-house	Viscous	No	k-ω SST	8.5×10^6	ALM	2
3	LES	Open-source	Inviscid	Wall func.	Smagor.	20×10^6	ALM (100)	3
4	LES	In-house	Inviscid	No	Smagor.	120×10^6	ALM (64)	5
5	LES	Open-source	Inviscid	Yes	Smagor.	28×10^6	ALM (108)	4

4. Phase I – Preliminary Results

The simulated results from the scientific community were compared against the experimental measurements conducted at TUM for two different scenarios, both including two wind turbines in tandem configuration: Case 1 involves the assessment of an upstream wind turbine with variable rotational speed, while the downstream wind turbine rotates at a designated rate. Case 2 is the exact opposite, with the upstream model operating at fixed rpm and the downstream one at variable rotational speed.

Figure 5 shows the coefficient of power, C_P, and the coefficient of thrust, C_T, over the Tip Speed Ratio (TSR) for the upstream wind turbine model. *Participant 1* successfully captures the power output throughout the majority of the curve, but they massively underpredict the power at $\mathrm{TSR} = 10$, showcasing a sudden drop of the computational curve. *Participant 3* tends to overpredict the power output by a considerable margin in high TSRs, even surpassing Betz's limit of $C_{P_{max}} = 0.593$. However, since the measurements were not corrected for blockage, such results can possibly be expected. *Participants 2 and 4* provide an excellent correlation with the experimental curve, only slightly deviating from the measurements. Finally, *Participant 5*'s single contribution correlates well with the experiment, showcasing a relative difference of just 5.8%.

As far as thrust is concerned, all contributors seem to consistently underpredict C_T for TSR values below approximately 6. However, from that point onwards, the simulated results from *Participants 1, 2* and *3* exhibit a considerable overprediction, indicating that the computational models may introduce a systematic deviation. Once again, *Participants 4* and *5* exhibit high levels of accuracy compared to the experiment.

As expected, predicting the performance of the tandem turbine proved to be a more demanding task. As depicted in Figure 6, *Participant 1* manages to predict the relative differences, while having a constant deviation from the experiment, taking into consideration that the case referring to $\mathrm{TSR} = 6$, is a possible outlier. The same applies to Participant 3, while Participant 2 shows a continuous descent as the TSR increases. However, the global minimum observed in the experimental curve within the range $\mathrm{TSR} \in (8, 9)$ cannot be clearly identified. Finally, *Participants' 4* and *5* predictions are the most accurate, with the latter's contribution deviating from the measurement by only 6.9% or 0.01 in absolute difference.

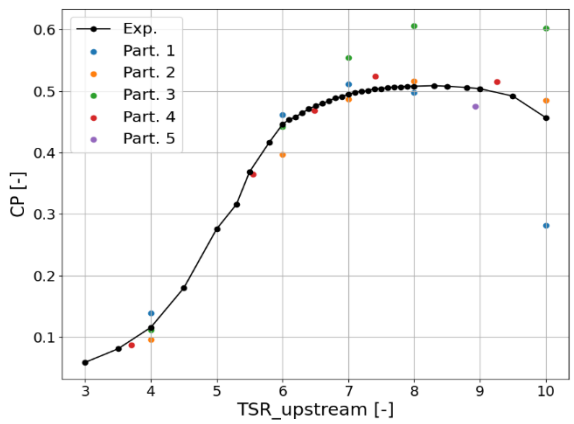

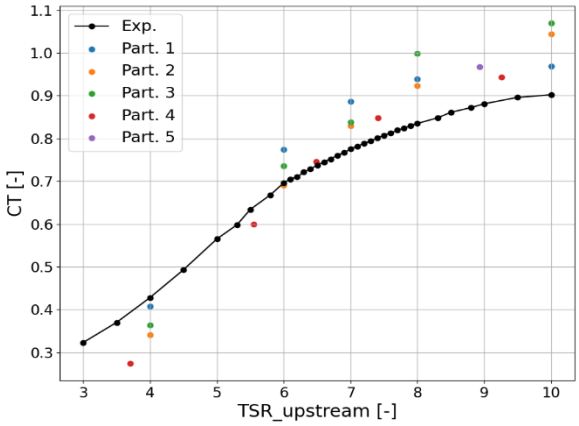

Figure 5. Phase I results – numerical approaches versus experimental measurements. Case 1 Upstream Wind Turbine. Coefficient of Power C_P (left) and Thrust C_T (right) versus the Tip Speed Ratio (TSR).

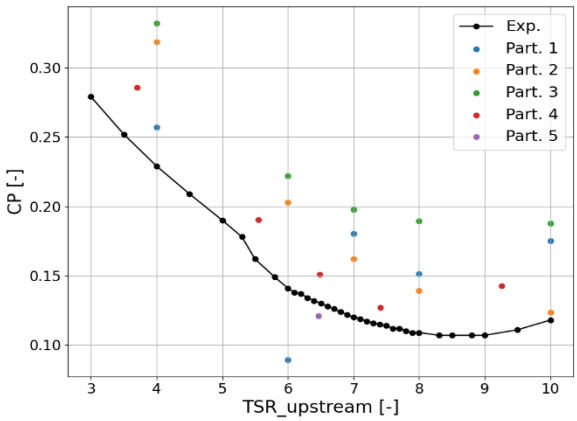

Figure 6. Phase I results – numerical approaches versus experimental measurements. Case 1 – Downstream Wind Turbine. C_P versus TSR.

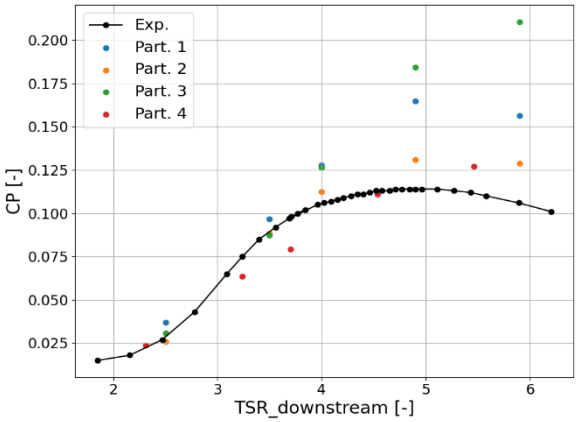

Figure 7. Phase I results – numerical approaches versus experimental measurements. Case 2 – Downstream Wind Turbine. C_P versus TSR.

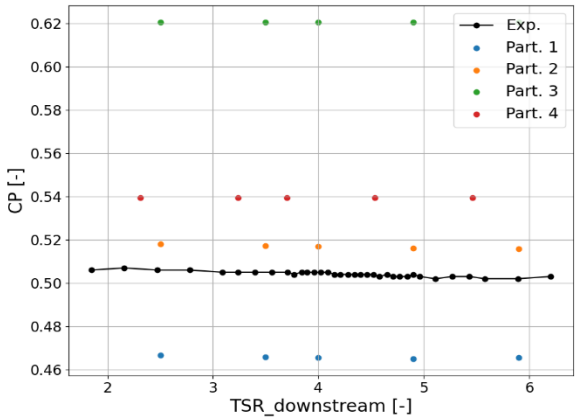

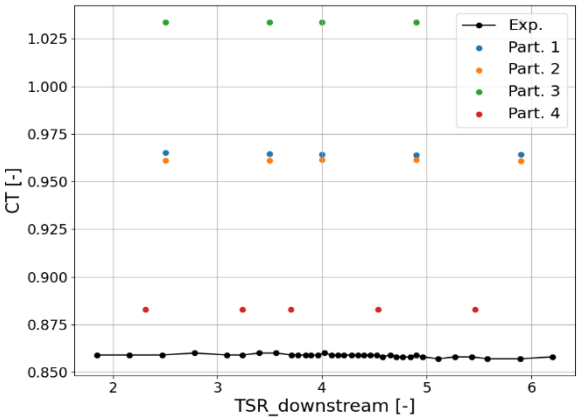

Figure 8. Phase I results – numerical approaches versus experimental measurements. Case 2 Upstream Wind Turbine. C_P (left) and C_T (right) versus the TSR.

Figure 8 illustrates the comparison between the experiment and the computational models for the upstream wind turbine of Case 2. In both cases, the numerical simulations manage to predict the relatively consistent performance of the turbine, albeit with a constant deviation from the measurement curve. Finally, Figure 7 shows the comparison for Case 2 for the downstream

turbine. Although *Participant 4* closely predicts the measurements, it is evident that the curve's trend is not captured, as the computational results show a continuous increase in power as the TSR grows. *Participants 1* and *2* do capture this reduction in power, however they misjudge the relative differences by a considerable margin. Finally, *Participant 3* fails to capture the experimental curve, exhibiting a totally unexpected result. Wake comparisons as well as more detailed analysis will be presented during the WAKE Conference.

5. Phase II

Phase II measurements emphasized wake control using individual blade pitch on the upstream turbine, along with a comparative analysis of numerical simulations and experimental results using metrics such as power coefficients, thrust coefficients, and wake characteristics.

5.1 Conditions

Phase II experiments were carried out in the large section $2.5 \times 3.5 \times 12\ m^3$ (H × W × L) of the closed-circuit wind tunnel at NTUA. The set up consists of two identically scaled wind turbine models which are placed in line with a longitudinal distance of 5D, see Figure 9. The inflow profile for Phase II was measured using a TSI Inc. IFA 300 measurement system with a single wire probe (TSI 1201), that was calibrated in-situ prior to the measurements. The sampling frequency was 10 kHz with a low pass filter at 5 kHz and a sampling time of 104 sec. For the calibration function, a 4th order polynomial was used and a temperature correction according to the manufacturer was applied. Both low turbulence (T. I. ≈ 1.5%) and high turbulence (T. I. ≈ 6%) inflow conditions were tested. The latter was achieved by adding a passive turbulence grid at the test section inlet. The grid comprised of wooden bars with a cross section of 24 mm × 48 mm, while the distance between the centres of the bars was 30 cm. The inflow conditions for both low and high turbulence intensity are given from two graphs in Figure . The first one refers to the longitudinal velocity component U_x normalized by the velocity at the hub height and the second one refers to the TI.

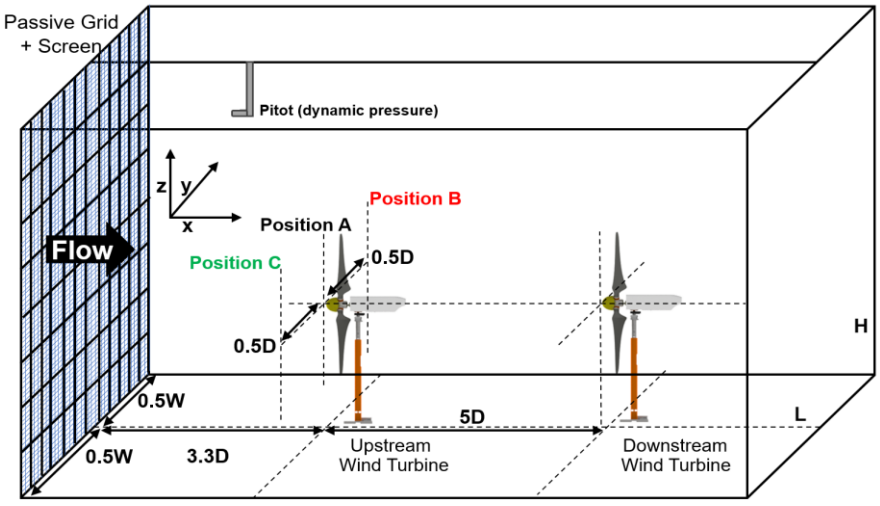

Figure 9. Sketch of the NTUA wind tunnel test section with the location of the pitot tube and the locations of the upstream and downstream wind turbine models.

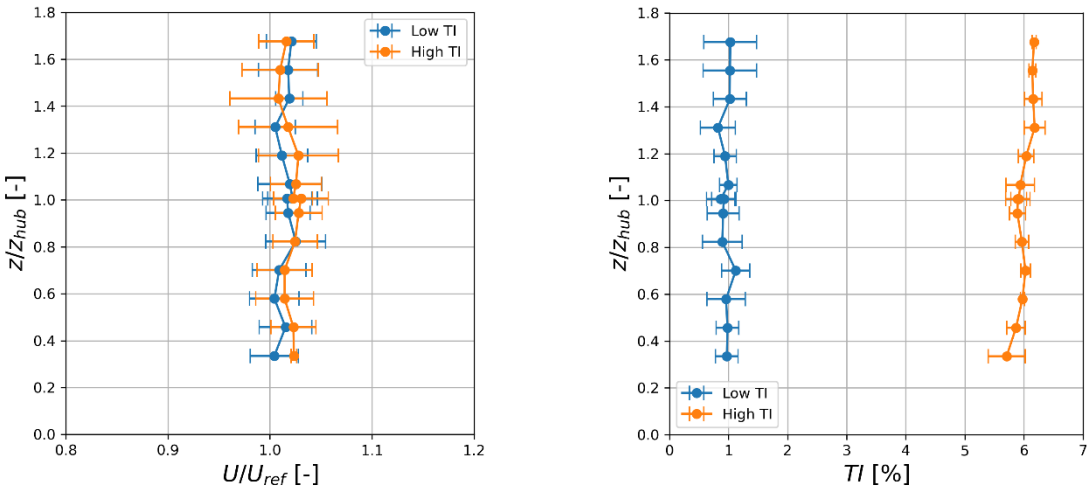

Figure 10. Normalized velocity (left) and turbulence intensity (right) per normalized height for the Low and High Turbulence Intensity configurations at NTUA.

In the context of Phase II, the upstream turbine was initially tested in its baseline configuration before being subjected to dynamic helix motion, with amplitude ranges of 3° and helix frequency of $f_{helix} = \frac{f_\beta}{f_r} \in [0.7,1.3]$, where $f_\beta = f_r \pm f_e$ represents individual sinusoidal blade excitation frequency, $f_r = 1P$ is the rotational frequency and f_e is the additional excitation frequency, which is either added to or subtracted from the rotational frequency, leading to the CCW or CW wake meandering, respectively [13]. The helix frequency range was determined based on the findings of [13], [14] which highlight the presence of two local optima in each meandering category, indicating an intriguing assymetry that warrants further measurement. Particle Tracking Velocimetry (PTV) measurements were also conducted within the context of Phase II, in a specified dimensionless helix frequency of $f_{helix} = 0.82$.

Table 2. List of experimental measurements of Phase II.

Case Number	Inflow	Configuration	Distance	Helix Amplitude [°]	f_{helix}
1	Low Turbulence	Baseline	5D	-	-
2	Low Turbulence	Helix	5D	3	[0.7,1.3]
3	High Turbulence	Baseline	5D	-	-
4	High Turbulence	Helix	5D	3	[0.7,1.3]

6. Conclusions

This paper presents an overview of the two-phase blind test initiative designed to advance wake modelling and control in wind energy research. Preliminary results from Phase I highlight the challenges in accurately capturing wake dynamics and turbine performance. While some participants achieve high accuracy in their predictions, systematic deviations, such as overprediction of power coefficients at high tip speed ratios and misalignment of the simulated thrust coefficients, were observed across some contributions.

The analysis of the simulation results shows the greater difficulty in accurately predicting the performance of downstream turbines compared to their upstream counterparts. This challenge

was expected, as downstream turbines operate within the wake of the upstream device, therefore the flow field is highly complex and characterized by turbulent structures, velocity deficits, and increased unsteadiness. Accurately defining the inflow conditions at the inlet of the tandem model becomes particularly challenging in this context, and definitely plays a pivotal role in result accuracy. Phase II of the blind test campaign offers a unique opportunity to deepen our understanding of helix-based wake control strategies, presenting computational modellers with a significantly more challenging task.

Acknowledgements

The authors kindly acknowledge the financial support of the European project 'TWEET-IE' funded by the European Union's Horizon 2020 Research and Innovation Programme (Grant Agreement 101079125).

References

[1] J. Meyers et al., "Wind farm flow control: prospects and challenges," Wind Energy Science, vol. 7, no. 6, pp. 2271–2306, Nov. 2022, doi: 10.5194/wes-7-2271-2022.

[2] P. Veers et al., "Grand challenges in the science of wind energy," Science (1979), vol. 366, no. 6464, Oct. 2019, doi: 10.1126/science.aau2027.

[3] P.-Å. Krogstad and P. E. Eriksen, "'Blind test' calculations of the performance and wake development for a model wind turbine," Renew Energy, vol. 50, pp. 325–333, Feb. 2013, doi: 10.1016/j.renene.2012.06.044.

[4] F. Mühle et al., "Blind test comparison on the wake behind a yawed wind turbine," Wind Energy Science, vol. 3, no. 2, pp. 883–903, Nov. 2018, doi: 10.5194/wes-3-883-2018.

[5] V. Pappa et al., "A blind test on wind turbine wake modelling based on wind tunnel experiments: Phase I – The benchmark case," J Phys Conf Ser, vol. 2767, no. 9, p. 092053, Jun. 2024, doi: 10.1088/1742-6596/2767/9/092053.

[6] C. Wang, F. Campagnolo, H. Canet, D. J. Barreiro, and C. L. Bottasso, "How realistic are the wakes of scaled wind turbine models?," Wind Energy Science, vol. 6, no. 3, pp. 961–981, Jun. 2021, doi: 10.5194/wes-6-961-2021.

[7] J. Katz and and A. Plotkin, "Low-Speed Aerodynamics, Second Edition," J Fluids Eng, vol. 126, no. 2, pp. 293–294, Mar. 2004, doi: 10.1115/1.1669432.

[8] J. G. Leishman, "Principles of helicopter aerodynamics," Cambridge University Press, 2000.

[9] J. N. Sørensen and W. Z. Shen, "Numerical Modeling of Wind Turbine Wakes," J Fluids Eng, vol. 124, no. 2, pp. 393–399, Jun. 2002, doi: 10.1115/1.1471361.

[10] H. Sarlak, C. Meneveau, and J. N. Sørensen, "Role of subgrid-scale modeling in large eddy simulation of wind turbine wake interactions," Renew Energy, vol. 77, pp. 386–399, May 2015, doi: 10.1016/j.renene.2014.12.036.

[11] M. J. Churchfield, S. J. Schreck, L. A. Martinez, C. Meneveau, and P. R. Spalart, "An Advanced Actuator Line Method for Wind Energy Applications and Beyond," in 35th Wind Energy Symposium, Reston, Virginia: American Institute of Aeronautics and Astronautics, Jan. 2017. doi: 10.2514/6.2017-1998.

[12] A. R. Meyer Forsting, G. R. Pirrung, and N. Ramos-García, "A vortex-based tip/smearing correction for the actuator line," Wind Energy Science, vol. 4, no. 2, pp. 369–383, Jun. 2019, doi: 10.5194/wes-4-369-2019.

[13] F. V. Mühle, F. M. Heckmeier, F. Campagnolo, and C. Breitsamter, "Wind tunnel investigations of an individual pitch control strategy for wind farm power optimization," Wind Energy Science, vol. 9, no. 5, pp. 1251–1271, May 2024, doi: 10.5194/wes-9-1251-2024.

[14] D. van der Hoek, B. Van den Abbeele, C. S. Ferreira, and J.-W. van Wingerden, "Maximizing wind farm power output with the helix approach -- experimental validation and wake analysis using tomographic PIV," Jun. 2023, [Online]. Available: http://arxiv.org/abs/2306.12849